A. Rivolta, P. Lunghi
Centralized/Decentralized Indirect Robust Adaptive Control for Spacecraft Attitude and Robotics
International Journal of Robust and Nonlinear Control, Vol. 33, N. 2, 2023, p. 933-952
doi:10.1002/rnc.6388

Centralized/Decentralized Indirect Robust Adaptive Control for spacecraft attitude and robotics

Aureliano Rivolta*[1] | Paolo Lunghi[2]

[1] D-Orbit SpA, Fino Mornasco, Italy
[2] Department of Aerospace Science & Technology, Politecnico di Milano, Milano, Italy

Correspondence
*Aureliano Rivolta, D-Orbit SpA, Viale Risorgimento, 57, 22073 Fino Mornasco (CO) - Italy. Email: aureliano.rivolta@dorbit.space

Summary

The diffuse presence of robotic subsystems in new space mission concepts introduces variations and uncertainties in system mass and inertia, imposing stringent constraints to orbital and attitude control. The required performance can be achieved through several paradigms like robust or adaptive controllers and sometimes a combination of the two. In this work, a novel indirect controller, belonging to the robust-adaptive controllers class, is developed, with the core idea of requiring just one adaptive gain with consequent lower sensitivity and easier tunability. The algorithm is developed both in centralized and decentralized formulation and tested for reliability and parameter sensitivity.

KEYWORDS:
Adaptive Control, Robust Control, Robotics, On Orbit Servicing

1 | INTRODUCTION

Space missions are increasingly becoming more elaborate and are going to require stringent performance in terms of control and robustness to disturbs and uncertainties, especially due to the presence of inherently variable systems such as robotic arms and tools[1]. The concepts of On-Orbit Servicing (OOS), miniaturization, and reusability of space assets are leading a change of paradigm in the space sector, which demands a even higher level of system autonomy and capability to react and adapt to different working conditions[2]. A typical example of such new scenarios is the case of a large carrier spacecraft with the task to release in different target orbits several passenger satellites[3,4]: at each release, mass and moment of inertia of the carrier suddenly change, with the system required to react without losses in pointing accuracy. The concept of OOS, in which a servicer spacecraft performs different tasks to prolong the lifetime of several target satellites, such as tugging, refueling, station keeping or even mechanical maintenance, requires the attitude control to be robust to a varying inertia in order to keep the system stable in all the different maneuvers: the servicer can acts alone or connected with the target, is required to perform complex grasping maneuvers to achieve connection, and it needs to handle the satellite stack even during mass transfers like refueling activities. The requested adaptability can be even greater, in case the properties of the target satellite are not fully known, or the connection between servicer and target is highly flexible, as it could be in an active debris removal mission[5].

From the perspective of industrial application, control laws shall be simpler and less elegant in order to be coded, tuned and verified with the required standards. Even though there exist several control paradigms that can theoretically achieve extreme performance, in many cases a simple PID architecture is deemed enough. A good example of optimal controller can be found in Reference [6] where the inverse optimal control paradigm is used to generate control laws that are optimal with respect to a certain cost function. In Reference [6] the inverse approach allows to skip the solution of a Hamilton-Jacobi equation. The resulting control law is complex and dependent on the model used for the synthesis, whereas PID like controllers require few weights to be set using certain paradigms: a possible way is to use H_∞[7] or μ synthesis[8] to account for uncertainties. The drawback of robust control is usually an augmented control effort, required to face a determined range of uncertainties. Hence, another way to face the problem is to use adaptive control theory, where the weights change according to an update law that compares the system response to a reference model that one wants to track. An example of adaptive control can be seen in Reference [9] or [10], which incorporates the estimation of the full inertia matrix that may result in excessive computations, especially since in the adaptive framework the convergence to true values is not guaranteed unless persistent excitation is exerted. Moreover, the estimation might be corrupted by measurement noises[11]. The adaptive approach can be extended to a variety of control paradigms, for example Reference [12] with a straightforward full inertia estimation is set to achieve optimality under the same premises of Reference [6]. An alternative approach consists in the estimation of the disturbances by a dedicated observer, that allows the controller to compensate as described in References [13] and [14].

Combining the robust approach and the adaptive approach is not easy but seems the logical answer to the problem. A interesting example of an elegant robust adaptive control can be found in Reference [15] although the tuning issue might presents. Robust adaptive controllers are generally not model-driven and are designed to face uncertainties or limitations in the control action[16,17,18,19]. The structure of the controller in Reference [15] is not conventional although resemble a proportional control: the problem lies in the variability of performance with the update gains. Several algorithms centered on robustness to actuation faults were investigated afterwards, often fusing adaptive backstepping and sliding modes[20,21,22,23,24,25] or following the original premises of Reference [15] like Reference [26]. On the other hand, finite time controllers like References [27,28] can attain good performance but requires more parameters to tune than Reference [15].

Should be noted that References [15,20,21,26] all suffer from the unwinding phenomena, which does not compromise stability but lower the performances. In general, we can intend fault tolerance to be tolerance to a certain level of input gain uncertainty and thus group many fault tolerant control in the greater scheme of control of uncertain systems.

The proportional feedback controls class is particularly attractive for space applications, for their implementation require very low computational power, a crucial aspect in a context in which computing capabilities are limited, especially in modern miniaturized systems. Taking inspiration from Reference [15] in this paper we present a new version of robust adaptive control which focuses on ease of tunability and predictability of the achievable performances. Such properties are particularly attractive for the practical implementation of space systems for they shorten development time, and they add strength to the verification process, a crucial phase of every mission. The version here expounded is tailored to the attitude control, although it can be extended to a larger class of problems. Since polynomials are involved, one might find a class of controllers resembling the approach of this paper in References [29,30] where a polynomial control law is determined through convex optimization. The control law is determined based on the model of the system, whereas here the assumptions on the knowledge of the system are quite relaxed.

The first major contribution is the theoretical development of the aforementioned controller, validated through extensive simulations, in which the control structure is simplified to make the tuning dependent on one single hyperparameter. While all the attractive features of previous works (simple implementation, adaptivity and robustness to failures and uncertainties) are retained, the tuning process to specific mission requirement is dramatically eased, shortening development activities. Moreover, the increased predictability of the achievable performances adds strength to the verification process, a crucial phase of the practical implementation of space missions. The formulation of the proposed algorithm retains sufficient generality to be extended beyond the original attitude control problem to complex robotic systems typical of the OOS context, although some limitations remains whenever different parts of the system are governed by very different dynamics. Such limitations are overcome by the second major finding of this work, which is the development of a decentralized version of the controller that can be better incorporated in the space robotics problem. Actuation fault and saturation of controls and parameters are also included in the assessment of a lightweight, robust and easily tunable algorithm. Performances and sensitivity to parameters are assessed through extensive simulations.

This paper is organized as follows. In Section 2 the attitude control problem, in terms of guidance to attain a certain attitude and in terms of dynamical response of a satellite angular velocities, is presented, along with its extension to the orbital robot case. Section 3 then presents the robust adaptive controller built upon the control problem of section 2. Extensive simulations of spacecraft attitude and robotics control scenarios are shown in Section 4 to highlight the potential of the proposed algorithm, while conclusions are drawn in Section 5.

2 | PROBLEM FORMULATION

The problem of controlling the attitude of a satellite can be divided in two concentric sub-problems: find the right velocity that would steer the attitude towards its goal and find the right torque to apply to the system in order to follow such velocity. If the second loop is faster than the first it is legit to separate the twos and analyze them separately.

This simplification can be accepted in most cases and helps maintaining the simplicity of the controllers and the grasp on the behavior of the system as a whole. More rigorous results could be achieved using a backstepping method like in References [31, 32], but the resulting controller would be more dependent on the model and have a more complex structure. Hence, here the separation approach is taken favoring simplicity of the complete control law.

First, the problem of finding the right velocity to be tracked will be briefly addressed, and the dynamical system to be controlled will be identified. Then, the classic attitude control system will be extended to the orbital robotics case, in which the spacecraft is distributed across relevant reconfigurable parts (i.e. a robotic arm) that shall be controlled, affecting the overall distribution of mass and inertia. A typical way to treat the rotational second order system is to use a backstepping procedure[6,33,12] leading to a complete controller, whose convergence cannot be global due to topological obstruction, hence only quasi-global asymptotical stability is achievable with continuous controllers[34,33,35]. A similar argument can be made for those controllers that use sliding modes instead of backstepping[16,17,18]. In this paper, the focus is put on the controller capabilities to overcome uncertainties and failures, regardless of the specific guidance law that would effectively track the desired attitude. This way of dealing with the attitude problem inherently assume full controllability of the system (using a reduced set of actuators would reduce the range of applicability or neglect it completely).

2.1 | Attitude guidance

The attitude of a rigid body needs to be parametrized in order to address the best strategy to achieve the desired pointing. Historically, quaternions have been used since are better suited to treat unconstrained rotations and are computationally friendly. Nevertheless, a quaternion $\mathbf{q}$ is composed by a real scalar part ε and an imaginary vector part $\boldsymbol{\eta}$ for a total of four elements. To map onto SO3, one needs to restrain quaternions to lie on the unitary sphere, hence $\mathbf{q}^T\mathbf{q} = \boldsymbol{\eta}^T\boldsymbol{\eta}+\varepsilon^2 = 1$. As a direct consequence there is a sort of duality where any attitude can be represented by $\mathbf{q}$ or $-\mathbf{q}$, leading to unwinding phenomena when trying to use $\mathbf{q}$ in a feedback loop.

Let us express the attitude error computed in controller frame using the error quaternion $\mathbf{q}_e$ and its components $\boldsymbol{\eta}_e$ and ε_e. The variation in time of the quaternion components in body axes can be expressed through the angular velocity of the reference attitude signal $\boldsymbol{\omega}_r$ and the current angular velocity of the body $\boldsymbol{\omega}_b$ as follows:

$$\begin{cases} 2\dot{\boldsymbol{\eta}}_e & = \boldsymbol{\eta}_e \times \left(\boldsymbol{\omega}_b + \boldsymbol{\omega}_r\right) + \varepsilon_e \left(\boldsymbol{\omega}_r - \boldsymbol{\omega}_b\right) \\ 2\dot{\varepsilon}_e & = \boldsymbol{\eta}_e^T \left(\boldsymbol{\omega}_b - \boldsymbol{\omega}_r\right) \end{cases} \tag{1}$$

Of the two possible solution families, $\mathbf{q}_0$ that represent null attitude error has $\varepsilon_0 = \pm 1$ and $\boldsymbol{\eta}_0 = \mathbf{0}$ with consequent $\boldsymbol{\omega}_b = \boldsymbol{\omega}_r$.

The ideal angular velocity reference $\boldsymbol{\omega}_{br}$ that drives $\mathbf{q}_e$ to the null quaternion $\mathbf{q}_0$ is given by:

$$\boldsymbol{\omega}_{br} = \beta \mathsf{s}\left(\varepsilon_e\right) \boldsymbol{\eta}_e + \boldsymbol{\omega}_r \tag{2}$$

with scalar parameter $\beta > 0$ and $\mathsf{s}\left(\varepsilon_e\right)$ a special function of the scalar element. This can be verified briefly through a simple Lyapunov analysis using a Candidate Lyapunov Function (CLF) $V_\varepsilon\left(\mathbf{q}_e\right)$ that is insensitive to quaternion sign change and is null for $\mathbf{q}_e = \mathbf{q}_0$:

$$\begin{aligned} V_\varepsilon\left(\mathbf{q}_e\right) &= \boldsymbol{\eta}_e^T \boldsymbol{\eta}_e = 1 - \varepsilon_e^2 && (3) \\ \dot{V}_\varepsilon\left(\mathbf{q}_e\right) &= -\varepsilon_e \boldsymbol{\eta}_e^T \left(\boldsymbol{\omega}_b - \boldsymbol{\omega}_r\right) && (4) \\ \boldsymbol{\omega}_b &\rightarrow \boldsymbol{\omega}_{br} \\ \dot{V}_\varepsilon\left(\mathbf{q}_e\right) &= -\varepsilon_e \beta \mathsf{s}\left(\varepsilon_e\right)\left(1 - \varepsilon_e^2\right) && (5) \end{aligned}$$

from which we can derive condition on $\mathsf{s}\left(\varepsilon_e\right)$: $\dot{V}_\varepsilon\left(\mathbf{q}_e\right) < 0\,\forall \mathbf{q}_e \iff \mathsf{s}\left(\varepsilon_e\right)\varepsilon_e > 0\,\forall \varepsilon_e \in [-1,\, 1]$. There is no continuous and limited function that can satisfy this property, hence we must use a discontinuous function that might introduce chattering or a discrete function updated using a threshold[35]. The first is a modified sign function:

$$\mathsf{s}\left(\varepsilon_e\right) = \begin{cases} 1 & \varepsilon_e \geq 0 \\ -1 & \varepsilon_e < 0 \end{cases} \tag{6}$$

while the second has $\mathsf{s}\left(\varepsilon_e\right) \rightarrow \mathsf{s}\left(\varepsilon_{e,z}\right) = h_z$ with discrete update given in Eq. (7), initial condition $h_0 = 1$ and a positive δ that sets a trade-off between robustness to noise and unwinding[35]:

$$h_{z+1} = \begin{cases} h_z & \varepsilon_{e,z} h_z \geq -\delta \\ -h_z & \varepsilon_{e,z} h_z < -\delta \end{cases} \tag{7}$$

The difference is noticeable only near $\varepsilon_e = 0$ where it has been shown that (7) outperforms (6)[35]. In both cases we have $\left|\mathsf{s}\left(\varepsilon_e\right)\right| = 1$ with $|\cdot|$ the absolute value of its argument. From this and the unitary condition follows that $\left\|\boldsymbol{\omega}_{br}\right\| \leq \beta + \left\|\boldsymbol{\omega}_r\right\|$.

2.2 Attitude dynamics

The attitude dynamics of a satellite can be represented by the Euler's equations expressed in a frame fixed with the rotating body as follows:

$$\dot{\boldsymbol{\omega}}_b = -\mathrm{I}_b^{-1}\dot{\mathrm{I}}_b\boldsymbol{\omega}_b - \mathrm{I}_b^{-1}\boldsymbol{\omega}_b \times \mathrm{I}_b\boldsymbol{\omega}_b + \mathrm{I}_b^{-1}\boldsymbol{\Gamma}\boldsymbol{\tau}_u + \mathrm{I}_b^{-1}\boldsymbol{\tau}_d \tag{8}$$

where I_b and $\boldsymbol{\omega}_b$are respectively the inertia tensor and the angular velocities expressed in body frame. External torques are divided in control $\boldsymbol{\tau}_u$ and disturbance $\boldsymbol{\tau}_d$ torques. The term $\dot{\mathrm{I}}_b$ takes into account geometrical variation of the system caused, for example, by a robotic appendage or fuel sloshing. Matrix $\boldsymbol{\Gamma}$ map the actuators' action on the system's degrees of freedom, and can include gains, actuator misplacement and other disturbs in the actuation line. In general it acts as the mapping between the commanded control action and the effective action applied to the system, and it depends on the specific system architecture. For example it can include the misalignment of a reaction wheel meaning that the control torque on one axis will have minor effects on another axis. In case of failure of one actuator, the mapping will be set to zero not allowing the intended control torque to reach the system. It is possible to use a simplified notation by setting the state of the system $\boldsymbol{x}$ equal to the angular velocity vector $\boldsymbol{\omega}_b$ and grouping together terms as follows:

$$\dot{\boldsymbol{x}} = \boldsymbol{A}\boldsymbol{x} + \boldsymbol{B}\boldsymbol{\tau}_u + g\left(\boldsymbol{x}\right) + \boldsymbol{d} \tag{9}$$

where the matrix $\boldsymbol{B}$ is the linear mapping between the control action and system dynamics. Such matrix is defined as the product of a positive definite matrix and the matrix $\boldsymbol{\Gamma}$ which in general is time dependent and non-symmetric:

$$\boldsymbol{B} = \mathrm{I}_b^{-1}\boldsymbol{\Gamma} \tag{10}$$

In Eq. (9) it has been set $\boldsymbol{A} = -\mathrm{I}_b^{-1}\dot{\mathrm{I}}_b$ and $g\left(\boldsymbol{x}\right) = -\mathrm{I}_b^{-1}\boldsymbol{\omega}_b \times \mathrm{I}_b\boldsymbol{\omega}_b$. These are respectively the linear dependency of the state dynamics from the state vector and the general non-linear state dependent contribution to the system dynamics. Going back to the actuation mapping, we can further specify $\boldsymbol{\Gamma}$ also in case of redundant actuation as follows:

$$\boldsymbol{\Gamma} = \boldsymbol{H}_{\boldsymbol{u}\boldsymbol{\Gamma}}\boldsymbol{\Gamma}_n\boldsymbol{H}_{\boldsymbol{\Gamma}\boldsymbol{u}} \tag{11}$$

where we have introduced $\boldsymbol{H}_{\boldsymbol{u}\boldsymbol{\Gamma}}$ as the linear map that convert the input of a set of n actuators into the dynamical system. On the other hand, $\boldsymbol{H}_{\boldsymbol{\Gamma}\boldsymbol{u}}$ is the matrix that maps the desired control action to a signal for each actuator and is commonly taken by control designers as the pseudoinverse of $\boldsymbol{H}_{\boldsymbol{u}\boldsymbol{\Gamma}}$ which is architecture/hardware dependent. $\boldsymbol{\Gamma}_n$ can be seen as the matrix that takes into account faults in actuators: in nominal conditions $\boldsymbol{\Gamma}_n = \mathbb{I}_{n\times n}$ where n is the number of actuators. In case of complete fault of the

ith actuator, the $\Gamma_{n\,i}$ element on the matrix diagonal is set to zero; partial degradation of the actuation action can be modeled with $0 < \Gamma_{n\,i} < 1$.

To better view the tracking problem, let us reason in terms of error $\boldsymbol{e}$ seen as the difference between a reference $\boldsymbol{r}$ and the state, $\boldsymbol{e} = \boldsymbol{r} - \boldsymbol{x}$, from which we can also compute error derivative with respect to time:

$$\dot{\boldsymbol{e}} = \dot{\boldsymbol{r}} - \boldsymbol{B}\boldsymbol{\tau}_u - \boldsymbol{A}\boldsymbol{x} - g\left(\boldsymbol{x}\right) - \boldsymbol{d} \tag{12}$$

Real satellite control must be designed taking into account different non-ideal conditions, among those we have control saturation, actuation fault, digital implementation, navigation errors, etc.

The non linear term $g\left(\boldsymbol{x}\right)$ has substantial influence when the reference angular velocity is non-zero and can cause divergence in simple control laws for higher errors. It can be shown that its gross influence depends on the error and its square as follows:

$$\left\|g\left(\boldsymbol{x}\right)\right\| \leq \sqrt{2}\left\|\mathrm{I}^{-1}\right\|_F \left\|\mathrm{I}\right\|_F \left(\left\|\boldsymbol{r}\right\|^2 + \left\|\boldsymbol{e}\right\|^2 + 2\left\|\boldsymbol{r}\right\|\left\|\boldsymbol{e}\right\|\right) \tag{13}$$

where it has been used the L2 vector norm $\|\cdot\|$ and the Frobenius norm $\|\cdot\|_F$ to maximize its influence. A similar consideration has been used in Reference [15] in terms of state vector norm. The optimal reference velocity that drives the attitude error to zero is given in Eq. (2), hence $\boldsymbol{r} = \boldsymbol{\omega}_{br}$ and $\|\boldsymbol{r}\| \leq \beta + \left\|\boldsymbol{\omega}_r\right\|$, thus if we limit the maximum $\left\|\boldsymbol{\omega}_r\right\|$ we limit also $\|\boldsymbol{r}\|$.

2.3 | Extension to space robotic problem

The dynamics presented in Sec. 2.2 describing a rigid body subject to control and disturbance toques, and to inertia variations, can be extended to include large, reconfigurable appendages capable to be controlled. A relevant example of such system is an orbital robot where a base satellite whose attitude can be described by quaternion $\mathbf{q}_b$ and angular velocity $\boldsymbol{\omega}_b$ which carries a robotic manipulator with revolute joints state $\boldsymbol{\vartheta}$. The model in this case would be:

$$\begin{bmatrix} \boldsymbol{M}_{\vartheta\vartheta} & \boldsymbol{M}_{\vartheta\mathbf{q}} \\ \boldsymbol{M}_{\mathbf{q}\vartheta} & \boldsymbol{M}_{\mathbf{q}\mathbf{q}} \end{bmatrix} \frac{d}{dt}\begin{Bmatrix} \dot{\boldsymbol{\vartheta}} \\ \boldsymbol{\omega}_b \end{Bmatrix} = \boldsymbol{d}\left(\boldsymbol{\vartheta}, \dot{\boldsymbol{\vartheta}}, \boldsymbol{\omega}_b, \mathbf{q}_b\right) + \boldsymbol{u} \tag{14}$$

where in matrix $\boldsymbol{M}_{\mathbf{q}\vartheta}$ and its transpose $\boldsymbol{M}_{\vartheta\mathbf{q}}$ are considered all terms that provide direct coupling between the base motion and the arm motion. The model can be directly adopted to formulate a control in a centralized fashion. Nevertheless, such type of control, for example based on the generalized Jacobian principle[36] or similar free floating algorithms, requires a very detailed knowledge of the system, and possibly other methods to increase robustness: couplings between system parts are non constant in time, and joints on manipulators are usually controlled in a decentralized way. Hence, the practical realization of such a control can be hard to achieve. On the other way round, a decentralized formulation would allow to attain good performance, still maintaining a certain ease of formulation by breaking down the system into manageable subproblems which are only weakly related to each other and can be solved independently[37,38]. This is particularly evident in the case in which different parts of the systems are characterized by very different dynamics, i.e. in case of very different moment of inertia, like the case of a robotic manipulator attached to a much more massive main body.

In the following Section, a new indirect robust adaptive controller is formulated in both centralized and decentralized version.

3 | CONTROL FORMULATION

3.1 | Feedback control

Taking into account the passivity considerations of the attitude control problem[39], a proportional velocity feedback control law is the simplest that can be implemented. Velocity-free controllers are not considered here. Taking into account a feedforward term for a generic time varying reference signal we have the following control law:

$$\boldsymbol{\tau}_u = \boldsymbol{K}\left(\boldsymbol{\lambda} \odot \boldsymbol{e} + \dot{\boldsymbol{r}}\right) \tag{15}$$

where $\boldsymbol{\lambda}$ is a vector of cutoff frequencies for the angular velocity loop, $\odot$ denotes the Hadamard product, and $\boldsymbol{K}$ is the feedback proportional gain matrix whose generic component is indicated with k_i. $\boldsymbol{K}$ can be determined to enforce $\boldsymbol{BK}$ to be positive definite, however this might be subject to uncertainties in the determination of $\boldsymbol{B}$ or its changes during the mission. In dynamical inversion controllers we have $\boldsymbol{K} \simeq \boldsymbol{B}^{-1}$ and thus $\dot{\boldsymbol{e}} = -\boldsymbol{\lambda} \odot \boldsymbol{e} - \boldsymbol{Ax} - g\left(\boldsymbol{x}\right) - \boldsymbol{d}$ which is asymptotically converging to zero only on special cases and with no disturbances. Since terms due to inertia variation and non linear cross coupling depends on the state, this control law is not able to guarantee convergence in all the error space. In fact, taking the following CLF:

$$V_{\varpi_0}\left(\boldsymbol{e}, \boldsymbol{x}\right) = \frac{1}{2}\boldsymbol{e}^T\boldsymbol{e} \tag{16}$$

we have a derivative that is:

$$\dot{V}_{\varpi_0}\left(\boldsymbol{e}, \boldsymbol{x}\right) = -\underbrace{\boldsymbol{e}^T\boldsymbol{\lambda} \odot \boldsymbol{e}}_{\geq 0} - \boldsymbol{e}^T\left(\boldsymbol{Ax} + g\left(\boldsymbol{x}\right) + \boldsymbol{d}\right) \tag{17}$$

which in general is not always negative definite. The only thing that we can assume about the disturbing terms is some sort of upper limit in the magnitude. In fact, exogenous disturbances to a spacecraft attitude are mainly due to atmospheric drag (if the satellite is in low Earth orbit), solar radiation pressure, magnetic field interaction with satellite dipole and non uniformity of the gravity field. Since such disturbance torques depend on the interaction of the external environment with inherently limited features of the spacecraft (ballistic coefficient, velocity, residual electric dipole, and moment of inertia), it is reasonable to assume them as bounded[40]. For what concern endogenous disturbances, they arise mainly due to effect such as actuators imprecision or misalignment, the presence of flexible appendages, fuel sloshing, mass depletion due to fuel consumption, and moving parts. Most of these quantities are characterized before launch, with mass and vibration tests. Several empirical models are commonly adopted to characterize sloshing as well[41,42], while effects like mass depletion and moving parts are limited by the performance of propulsion systems and robotic masses and actuators. Hence, we can reasonably assume that $\boldsymbol{d}$ has bounded modulus, $\|\boldsymbol{A}\|_F$ is upper bounded, and that the reference signal and its derivative are bounded. The latter poses limits to attitude tracking, basically putting an upper limit on the bandwidth of the complete controller.

The controller presented in Reference [15] is the most prominent controller of the proportional velocity feedback control class and was used here as a starting point to deliver a novel adaptive robust controller that guarantees stability, performance and is easy to tune.

In Reference [15] $\boldsymbol{K} = k\mathbb{I}_{3\times 3}$ where the scalar variable k is updated through a non straightforward but Lyapunov stable law function of the norm of the state and the error. The control law is summarized in Eq. (18) with a little modification from the original implementation to take into account $\boldsymbol{\lambda}$ and the feedforward $\dot{\boldsymbol{r}}$, and a slightly modified notation to uniform to convention adopted in this work:

$$\begin{cases} \boldsymbol{\tau}_u = k\left(\boldsymbol{\lambda} \odot \boldsymbol{e} + \dot{\boldsymbol{r}}\right), & k = \left(\upsilon_0 + \delta_\upsilon\right) \\ \delta_\upsilon = \frac{\hat{b}\Phi}{\|e\|+\epsilon}, & \Phi = 1 + \|\boldsymbol{x}\| + \|\boldsymbol{x}\|^2 \\ \dot{\hat{b}} = -\sigma_1 \hat{b} + \sigma_2 \frac{\|e\|^2\Phi}{\|e\|+\epsilon}, & \epsilon = \frac{\mu}{1+\Phi} \end{cases} \tag{18}$$

where δ_υ, $\hat{b}$, and Φ are intermediate quantities with no physical meaning, designed to achieve a self stiffening controller that guarantees bounded convergence[15]. In spite of this very attractive feature, the implementation is not straightforward, as it depends by the tuning of the three independent parameters $\left(\sigma_1, \sigma_2, \mu\right) > 0$ that might cause a lack of robustness with respect to the gains. On the other hand, the main feature of this algorithm is the error convergence to a very small boundary that depends mainly on the combination of parameters and upper boundaries on the disturbing terms as previously explained.

The controller of Eq. (18) will be referred to as Indirect Robust Adaptive Control (IRAC) for any following reference.

3.2 | Centralized robust controller

In order to avoid gain sensitivity it is possible to derive a similar controller adopting a simplified structure, with the advantage that only one parameter is left to be tuned. Let us take a centralized controller with scalar proportional term k as follows:

$$\boldsymbol{\tau}_u = k\left(\boldsymbol{\lambda} \odot \boldsymbol{e} + \dot{\boldsymbol{r}}\right) \tag{19}$$

$$k = \left(\|\boldsymbol{e}\| + 1\right) f \tag{20}$$

Then take the CLF[15]:

$$V_1\left(\boldsymbol{e},\, f\right) = \frac{1}{2}\boldsymbol{e}^T\boldsymbol{e} + \frac{1}{2\gamma_r h}\left(C - hf\right)^2 \tag{21}$$

where $\boldsymbol{C}$ is a finite positive constant scalar entity that must satisfy few conditions that will be introduced later. f is a time varying positive parameter, $\gamma_r > 0$ a constant, and $h > 0$ is the minimum influence of the control torques to the system.

Let us derive w.r.t. time (21) and substitute (12) and (19):

$$\begin{aligned}\dot{V}_1\left(\boldsymbol{e},\, f\right) =& - k\boldsymbol{e}^T\boldsymbol{B}\mathrm{diag}\left(\lambda\right)\boldsymbol{e} + \left(C - hf\right)\left(-\frac{\dot{f}}{\gamma_r}\right)\\ &+ \boldsymbol{e}^T\left(\left(\mathbb{I}_{3\times3} - \boldsymbol{B}k\right)\dot{\boldsymbol{r}} - \boldsymbol{A}\boldsymbol{x} - g\left(\boldsymbol{x}\right) - \boldsymbol{d}\right)\end{aligned} \tag{22}$$

Then we substitute the relation between k and f of (20) and determine a scalar valued function greater than the CLF derivative as follows.

$$\begin{aligned}\dot{V}_1\left(\boldsymbol{e},\, f\right) \leq& - \left(\|\boldsymbol{e}\|^2 + \|\boldsymbol{e}\|^3\right)hf + \left(C - hf\right)\left(-\frac{\dot{f}}{\gamma_r}\right)\\ &+ \|\boldsymbol{e}\|\left\|\left(\mathbb{I}_{3\times3} - \boldsymbol{B}k\right)\dot{\boldsymbol{r}} - \boldsymbol{A}\boldsymbol{x} - g\left(\boldsymbol{x}\right) - \boldsymbol{d}\right\|\end{aligned} \tag{23}$$

In Eq. (23) we have taken the highest possible value for the scalar products of disturbing elements and the minimum control influence over the CLF derivative.

For the latter it has assumed that exists a h such as $\boldsymbol{e}^T\boldsymbol{B}\mathrm{diag}\left(\lambda\right)\boldsymbol{e} > h\,\|\boldsymbol{e}\|^2$. This is always true for a positive definite matrix (symmetry is not required, this poses some limits on λ). h constitutes de facto the minimum influence of the controller onto the system and it is closely related to the controllability of the system. The only requirement for this proof is that h is a strictly positive value, which implies that the system must be controllable. A simple example of this would be a case where $\boldsymbol{\Gamma}_n$ of Eq. (11) has rank lower than three: there are not enough actuators to fully control the system and h would be null. Same effect would be caused by inverted signs in the actuators, where h would be negative and the controller would not be able to recover.

A term for sure larger than the disturbing components can be also found, leaving a direct dependency on $\|\boldsymbol{e}\|$:

$$\dot{V}_1\left(\boldsymbol{e},\, f\right) \leq -\left(\|\boldsymbol{e}\|^2 + \|\boldsymbol{e}\|^3\right) hf + \left(C - hf\right)\left(-\frac{\dot{f}}{\gamma_r}\right) + C_1\,\|\boldsymbol{e}\| + C_2\,\|\boldsymbol{e}\|^2 + C_3\,\|\boldsymbol{e}\|^3 \tag{24}$$

where the coefficients C_1, C_2 and C_3 are given by:

$$\begin{cases} C_1 & = \|\dot{\boldsymbol{r}}\|_{\mathrm{M}} + \|\boldsymbol{A}\|_F\,\|\boldsymbol{r}\|_{\mathrm{M}} + C_3\,\|\boldsymbol{r}\|_{\mathrm{M}}^2 + \|\boldsymbol{d}\|_{\mathrm{M}} \\ C_2 & = \|\boldsymbol{A}\|_F + 2C_3\,\|\boldsymbol{r}\|_{\mathrm{M}} \\ C_3 & = \sqrt{2}\left\|\mathrm{I}^{-1}\right\|_F\,\|\mathrm{I}\|_F \end{cases} \tag{25}$$

where with $\|\cdot\|_{\mathrm{M}}$ is intended the maximum value the norm of the argument can take. It is possible to increase the second and third order disturbs as follows:

$$C\left(\|\boldsymbol{e}\| + \|\boldsymbol{e}\|^2 + \|\boldsymbol{e}\|^3\right) > \mathbb{P}_C^3\left(\|\boldsymbol{e}\|\right) \tag{26}$$

$$\mathbb{P}_C^3\left(\|\boldsymbol{e}\|\right) = C_1\,\|\boldsymbol{e}\| + C_2\,\|\boldsymbol{e}\|^2 + C_3\,\|\boldsymbol{e}\|^3 \tag{27}$$

where $\mathbb{P}_i^n\left(\|\boldsymbol{e}\|\right)$ represent the polynomial i of order n in the scalar abscissa $\|\boldsymbol{e}\|$. This relation becomes de facto the definition of the constant C, implying $C \geq C_1$, $C \geq C_2$, and $C \geq C_3$.

This leads to:

$$\dot{V}_1\left(\boldsymbol{e},\, f\right) \leq C\,\|\boldsymbol{e}\| + \left(C - hf\right)\left(\|\boldsymbol{e}\|^2 + \|\boldsymbol{e}\|^3\right) + \left(C - hf\right)\left(-\frac{\dot{f}}{\gamma_r}\right) \tag{28}$$

$\dot{f}$ can be expanded as in Eq. (29), in this case the second and third order effects would be removed but no conclusion on the CLF derivative sign can be made as it would be generally lower than $C\,\|\boldsymbol{e}\|$.

$$\dot{f} = \gamma_r\left(\|\boldsymbol{e}\|^2 + \|\boldsymbol{e}\|^3\right) \tag{29}$$

This deviation was intended to show the definition of C that lead to Eq. (29). Going back few steps and leaving second and third order terms leads to a different conclusion: substituting (29) in (24) leads to

$$\dot{V}_1(\boldsymbol{e}, f) \leq \mathbb{P}_1^3(\|\boldsymbol{e}\|) \tag{30}$$

$$\mathbb{P}_1^3(\|\boldsymbol{e}\|) = C_1\|\boldsymbol{e}\| + \left(C_2 - C\right)\|\boldsymbol{e}\|^2 + \left(C_3 - C\right)\|\boldsymbol{e}\|^3 \tag{31}$$

which is a third order polynomial with second and third order coefficients lower or equal to zero. It has only two admissible roots, $\|\boldsymbol{e}\|_1 = 0$ and $\|\boldsymbol{e}\|_2 > 0$. For any $\|\boldsymbol{e}\| > \|\boldsymbol{e}\|_2$ we will have $\dot{V}_1(\boldsymbol{e}, f) < 0$.

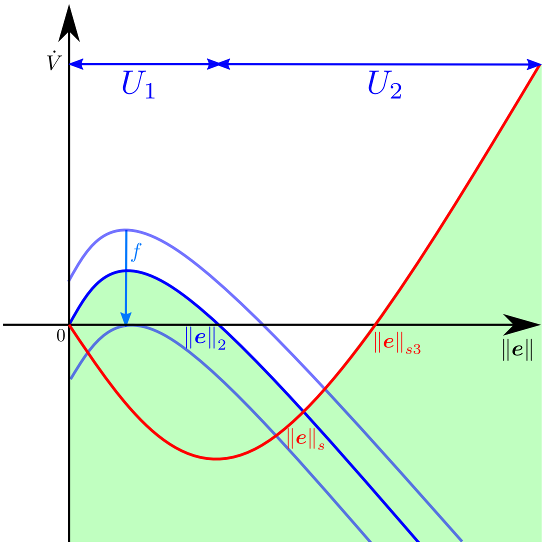

FIGURE 1 Lyapunov functions derivatives. The upper boundary of CIRAC $\dot{V}_1$, $\mathbb{P}_1^3(\|\boldsymbol{e}\|)$, is denoted in blue, red marks the derivative of a saturation control. The theoretical development of controllers does not take into account saturation: in real systems stability is limited by the available control authority, and the actual trend of the CLF derivative is the maximum of the two curves, highlighted by the green envelope. In light blue the trend of $\mathbb{P}_1^3(\|\boldsymbol{e}\|)$ as f increases is also shown.

In conclusion, this modification requires to tune only one gain γ_r. Figure 1 shows in blue the trend of $\mathbb{P}_1^3(\|\boldsymbol{e}\|)$ which constitutes the upper boundary for the CLF derivative $\dot{V}_1$. It can be seen how the error space can be divided in $U_1 = \left[\|\boldsymbol{e}\|_1, \|\boldsymbol{e}\|_2\right]$ where derivative of $V_1(\boldsymbol{e}, f)$ can be positive and a region $U_2 = \left[\|\boldsymbol{e}\|_2, \infty\right)$ where the derivative is always negative. Since in U_2 we have $\dot{V}_1(\boldsymbol{e}, f) < 0$ we can conclude that both $\boldsymbol{e}$ and f are limited. This behavior identifies a Uniform Ultimate Boundedness (UUB) convergence of controller (19) – (20) with update (29). For simulations, this controller will be indicated as Centralized Indirect Robust Adaptive Control (CIRAC).

In practice, control saturation imposes an upper threshold of convergence for reference tracking. The red curve in Figure 1 denotes the saturation curve, referred to a controller that outputs always the maximum torque with the proper sign: $\boldsymbol{\tau}_u = u_{\mathrm{m}}\mathrm{sign}(\boldsymbol{e})$ with $u_{\mathrm{m}} = \left\|\boldsymbol{\tau}_u\right\|_{\mathrm{M}}$. Such relation sets the theoretical highest action a real controller can provide, and its more evident practical consequence is that there exists an error upper boundary $\|\boldsymbol{e}\|_{s3}$ beyond which the real controller will not be able to recover, due to the limited available control authority. The overall behavior of a real controller would follow the maximum of the two curves, highlighted by the green envelope in the figure.

A possible drawback in this type of controller is the problem of gain saturation. As it is clear from (29), the parameter f can only grow in time and with a train of reference step functions it would saturate. A possible addition is a negative bias in (29) that would lower the value of f if the error goes below a certain threshold $\|\boldsymbol{e}\|_{\mathrm{M}}$.

$$\dot{f} = \gamma_r \left(\|\boldsymbol{e}\|^2 + \|\boldsymbol{e}\|^3\right) - \gamma_r \left(\|\boldsymbol{e}\|_{\mathrm{M}}^2 + \|\boldsymbol{e}\|_{\mathrm{M}}^3\right) \tag{32}$$

This does modify $\mathbb{P}_1^3\left(\|\boldsymbol{e}\|\right)$ by a zero order term $(C - hf)\left(\|\boldsymbol{e}\|_{\mathrm{M}}^2 + \|\boldsymbol{e}\|_{\mathrm{M}}^3\right)$ that can be considered a translating term for $\mathbb{P}_1^3\left(\|\boldsymbol{e}\|\right)$. Such term lowers the higher f becomes, and there is a theoretical value $\overline{f}$ for which $\dot{V}_1\left(\boldsymbol{e},\, \overline{f}\right) < 0\,\forall \boldsymbol{e}$. This theoretical value does not take into account saturation. If f grows it will reach inevitably a value for which $\|\boldsymbol{e}\| < \|\boldsymbol{e}\|_{\mathrm{M}}$ and its update would change sign; the velocity error settles approximately around $\|\boldsymbol{e}\|_{\mathrm{M}}$. In Figure 1, in light blue, it is possible to appreciate the vertical translation due to f and the consequent reduction of $\|\boldsymbol{e}\|_2$. This is intuitive as the increase in rigidity would reduce the final error bound.

The term hf would then theoretically settle at a value which is function of $\mathbb{P}_C^3\left(\|\boldsymbol{e}\|_{\mathrm{M}}\right)$ and $\|\boldsymbol{e}\|_{\mathrm{M}}$ as in the following equation:

$$hf|_{\mathrm{end}} \simeq \frac{\mathbb{P}_C^3\left(\|\boldsymbol{e}\|_{\mathrm{M}}\right)}{\|\boldsymbol{e}\|_{\mathrm{M}}^2 + \|\boldsymbol{e}\|_{\mathrm{M}}^3} \tag{33}$$

The order of magnitude of the controller gain γ_r can be roughly determined by settling the mean speed of update and the expected plausible errors.

3.3 | Decentralized robust controller

The previous centralized control can be adapted to work decentralized with few modifications. Let us take the control action to be:

$$\boldsymbol{\tau}_u = \boldsymbol{k} \odot (\boldsymbol{\lambda} \odot \boldsymbol{e} + \dot{\boldsymbol{r}}) \tag{34}$$

$$\boldsymbol{k} = |\boldsymbol{e}| \odot \boldsymbol{f} + \boldsymbol{f} \tag{35}$$

where it has been used $|\cdot|$ as the element-wise absolute value operator, such that all components of $|\boldsymbol{e}|$ are positive. In this specific case it has been used $\boldsymbol{k}$ to indicate a column vector made by three different k_i. A new CLF is determined from $V_1\left(\boldsymbol{e},\, f\right)$ with minor modification to comply with the increased dimension of f as:

$$V_2(\boldsymbol{e},\,\boldsymbol{f}) = \frac{1}{2}\boldsymbol{e}^T\boldsymbol{e} + \frac{1}{2\gamma_r h}\left(C\mathbf{1} - h\boldsymbol{f}\right)^T\left(C\mathbf{1} - h\boldsymbol{f}\right) \tag{36}$$

where with $\mathbf{1}$ we have denoted the vector made of ones on every axis. It is equivalent to state that each component of $\boldsymbol{f}$ should update according to a single C that is defined for the whole system. Then, substituting Eq. (34) and Eq. (35) and upper bounding the derivative of $V_2(\boldsymbol{e},\,\boldsymbol{f})$ like in the previous case leads to:

$$\begin{aligned}\dot{V}_2(\boldsymbol{e},\,\boldsymbol{f}) \leq & - h\boldsymbol{e}^T\mathrm{diag}(\boldsymbol{f})\,\boldsymbol{e} - h\boldsymbol{e}^T\left(\boldsymbol{e}\odot|\boldsymbol{e}|\odot\boldsymbol{f}\right)\\ & + \mathbb{P}^3_C(\|\boldsymbol{e}\|) + \left(C\mathbf{1} - h\boldsymbol{f}\right)^T\left(-\frac{\dot{\boldsymbol{f}}}{\gamma_r}\right)\end{aligned} \tag{37}$$

The decentralized update law of $\boldsymbol{f}$ can be written similarly as (29) or (32) but in a decentralized fashion.

$$\dot{\boldsymbol{f}} = \gamma_r\left(|\boldsymbol{e}|^2 + |\boldsymbol{e}|^3\right) \tag{38}$$

Then substituting Eq. (38) into Eq. (37) and writing in a concise way the first two terms leads to:

$$\dot{V}_2(\boldsymbol{e},\,\boldsymbol{f}) \leq -h\sum\left(\boldsymbol{f}\odot\left(|\boldsymbol{e}|^2 + |\boldsymbol{e}|^3\right)\right) + \mathbb{P}^3_C(\|\boldsymbol{e}\|) - \left(C\mathbf{1} - h\boldsymbol{f}\right)^T\left(|\boldsymbol{e}|^2 + |\boldsymbol{e}|^3\right) \tag{39}$$

Then, since it is clear that $\boldsymbol{f}^T\left(|\boldsymbol{e}|^2 + |\boldsymbol{e}|^3\right) = \sum\left(\boldsymbol{f}\odot\left(|\boldsymbol{e}|^2 + |\boldsymbol{e}|^3\right)\right)$ we reach the following result recalling Eq. (31):

$$\dot{V}_2(\boldsymbol{e},\,\boldsymbol{f}) \leq C_1\|\boldsymbol{e}\| + C_2\|\boldsymbol{e}\|^2 + C_3\|\boldsymbol{e}\|^3 - C\sum\left(|\boldsymbol{e}|^2 + |\boldsymbol{e}|^3\right) \tag{40}$$

where $\mathbf{1}^T\left(|\boldsymbol{e}|^2 + |\boldsymbol{e}|^3\right)$ is equal to the sum for all components/axis of $\left(|\boldsymbol{e}|^2 + |\boldsymbol{e}|^3\right)$. Now, let us upper bound $\mathbb{P}^3_C(\|\boldsymbol{e}\|)$ as follows by using $\sum(|\boldsymbol{e}|) \geq \|\boldsymbol{e}\|$, $\|\boldsymbol{e}\|^2 = \sum\left(|\boldsymbol{e}|^2\right)$, and $3\sqrt{3}\sum\left(|\boldsymbol{e}|^3\right) \geq \|\boldsymbol{e}\|^3$ that are valid for any $\boldsymbol{e}$:

$$\mathbb{P}^3_C(\|\boldsymbol{e}\|) \leq \mathbb{P}^3_{C'}(|\boldsymbol{e}|) \tag{41}$$

$$\mathbb{P}^3_{C'}(|\boldsymbol{e}|) = C_1\sum(|\boldsymbol{e}|) + C_2\sum\left(|\boldsymbol{e}|^2\right) + 3\sqrt{3}C_3\sum\left(|\boldsymbol{e}|^3\right) \tag{42}$$

$$\mathbb{P}^3_C(\|\boldsymbol{e}\|) \leq C\left(\sum(|\boldsymbol{e}|) + \sum\left(|\boldsymbol{e}|^2\right) + \sum\left(|\boldsymbol{e}|^3\right)\right) \tag{43}$$

from which follows:

$$\dot{V}_2(\boldsymbol{e},\,\boldsymbol{f}) \leq C_1\|\boldsymbol{e}\| + \left(C_2 - C\right)\sum\left(|\boldsymbol{e}|^2\right) + \left(3\sqrt{3}C_3 - C\right)\sum\left(|\boldsymbol{e}|^3\right) \tag{44}$$

Since the definition of C in Eq. (26) can imply $C > C_2$ and $C > 3\sqrt{3}C_3$ we can minimize the negative terms of Eq. (44) and arrive at:

$$\dot{V}_2\left(\boldsymbol{e},\,\boldsymbol{f}\right) \leq \mathbb{P}_2^3\left(\|\boldsymbol{e}\|\right) \tag{45}$$

$$\mathbb{P}_2^3\left(\|\boldsymbol{e}\|\right) = C_1\,\|\boldsymbol{e}\| + \left(C_2 - C\right)\|\boldsymbol{e}\|^2 + \left(C_3 - \frac{C}{3\sqrt{3}}\right)\|\boldsymbol{e}\|^3 \tag{46}$$

Like for the centralized case we have a third order polynomial $\mathbb{P}_2^3\left(\|\boldsymbol{e}\|\right)$ with second and third order coefficients negative. All the considerations made before still apply for the decentralized case. Adding the bias in the adaptive term update like in Eq. (47) allows to assure theoretically that $\boldsymbol{f}$ is bounded, as a pure translating term is added to $\mathbb{P}_2^3\left(\|\boldsymbol{e}\|\right)$ that lowers with $\boldsymbol{f}$ as shown in Eq. (48). Of course, with $|\boldsymbol{e}|_{\mathrm{M}}$ is intended the maximum allowable error per axis.

$$\dot{\boldsymbol{f}} = \gamma_r\left(|\boldsymbol{e}|^2 + |\boldsymbol{e}|^3\right) - \gamma_r\left(|\boldsymbol{e}|_{\mathrm{M}}^2 + |\boldsymbol{e}|_{\mathrm{M}}^3\right) \tag{47}$$

$$\dot{V}_2\left(\boldsymbol{e},\,\boldsymbol{f}\right) \leq \mathbb{P}_2^3\left(\|\boldsymbol{e}\|\right) + \left(C\mathbf{1} - h\boldsymbol{f}\right)^T\left(|\boldsymbol{e}|_{\mathrm{M}}^2 + |\boldsymbol{e}|_{\mathrm{M}}^3\right) \tag{48}$$

Due to its nature this algorithm can be called Decentralized Indirect Robust Adaptive Control (DIRAC). The difference with respect to the centralized controller is that each axis can work independently from the others. This feature may find limited uses in attitude control but allows for a practical extension to the orbital robot case. As far as attitude control is concerned, the difference lies in the fact that $\mathbb{P}_2^3\left(\|\boldsymbol{e}\|\right) \geq \mathbb{P}_1^3\left(\|\boldsymbol{e}\|\right)$ and that the final value of $h\,\|\boldsymbol{f}\|$ is approximately given by

$$h\,\|\boldsymbol{f}\|\,|_{\text{end}} \gtrsim \frac{\mathbb{P}_C^3\left(\left\||\boldsymbol{e}|_{\mathrm{M}}\right\|\right)}{\left\||\boldsymbol{e}|_{\mathrm{M}}^2 + |\boldsymbol{e}|_{\mathrm{M}}^3\right\|} \tag{49}$$

It is then obvious that such value can be greater than the value of CIRAC, thus it is generically expected to have higher expenses using DIRAC instead of CIRAC.

4 | NUMERICAL SIMULATIONS

In order to assess the performance, the robustness, and the ease of tuning of the proposed methods, a simulation campaign has been carried out and it is here presented. The first part is dedicated to the attitude control problem with comparison of different algorithms cited or presented in this work. Comparisons are made in terms of controller parameter sensitivity and in terms of initial attitude error. With the same model, also convergence claims of CIRAC are analyzed. In the second part, an implementation of the decentralized adaptive control applied to an orbital robotic case is studied.

4.1 | Attitude control

The test case sees a satellite with the following inertia matrix:

$$\mathrm{I} = \begin{bmatrix} 12.75 & 5.20 & -4.76 \\ 5.20 & 33.00 & -9.00 \\ -4.76 & -9.00 & 18.25 \end{bmatrix} \mathrm{kg\,m^2} \tag{50}$$

and with general properties listed in Table 1. This includes also attitude guidance parameters, kept constant for the comparison, and limits on the proportional gains of the controllers k_i. Such quantities are kept constant for every simulation. The values of the controller parameters, including the initial k_i values and other gains are listed in Table 2. Two different simulation campaigns are conducted to check initial condition and gain sensitivity of IRAC, CIRAC and DIRAC.

TABLE 1 Test case data.

Symbol	Value
u_m	$0.5\,\mathrm{Nm}$
λ	$\frac{1}{2}\mathbb{I}_{3\times3}$
β	0.05
k_i	$[0.1,\ 50]$
$\mathbf{q}_{r,0}$	$\begin{bmatrix}0 & 0 & 0.26 & 0.97\end{bmatrix}^T$
$\boldsymbol{\omega}_r$	$\begin{bmatrix}0 & 0.0010 & 0.0017\end{bmatrix}^T$
$\boldsymbol{d}$	$\begin{bmatrix}0 & 0 & 0\end{bmatrix}^T$
$\lVert\dot{\boldsymbol{r}}\rVert_\mathrm{M}$	$0.0002,\ ^{\mathrm{rad}}/_{\mathrm{s}^2}$
$\lVert\boldsymbol{r}\rVert_\mathrm{M}$	$0.02,\ ^{\mathrm{rad}}/_{\mathrm{s}}$

TABLE 2 Controllers data.

Controller	k_i	Other Gains
IRAC[15]	0.6375	$\begin{cases}\sigma_1 & = 0.01 \\ \sigma_2 & = 100 \\ \mu & = 0.1\end{cases}$
CIRAC	0.6375	$\gamma_a = 10^4$
DIRAC	0.6375	$\gamma_a = 10^5$

4.1.1 | Sensitivity to gain variation

To assess the system sensitivity to the variation of the gains a set of 1000 test cases has been run. In each simulation, the initial conditions (null attitude and rotational rate) and the target desired ones (Table 1) has been kept constant, while the "Other Gains" in Table 2 have been varied in each run by multiplication for a factor $10^{1.5\phi}$ with ϕ generated randomly with a uniform distribution in the range $[-1, 1]$.

The duration of the simulation is set to 1200 seconds, and at time $t = 600s$, a failure in a reaction wheel (it stops giving torque to the system) is simulated with an instantaneous change in $\boldsymbol{B}$ (which becomes also non-symmetric). A pyramid configuration of 4 reaction wheels is assumed. The reference is given by $\mathbf{q}_r$, updated with a constant angular velocity $\boldsymbol{\omega}_r$.

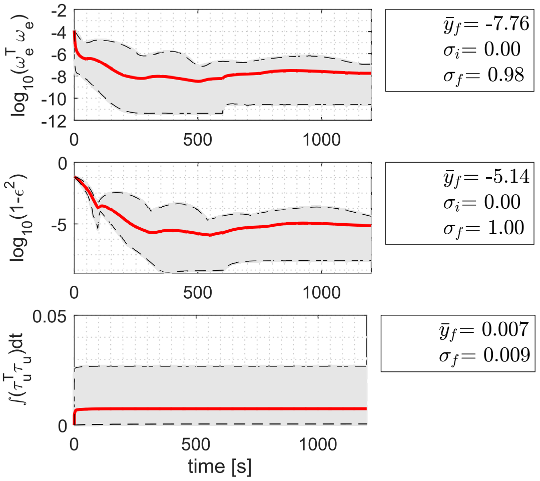

FIGURE 2 IRAC gain sensitivity. Dashed lines highlight the envelope of simulations, the red full lines indicate the mean curves.

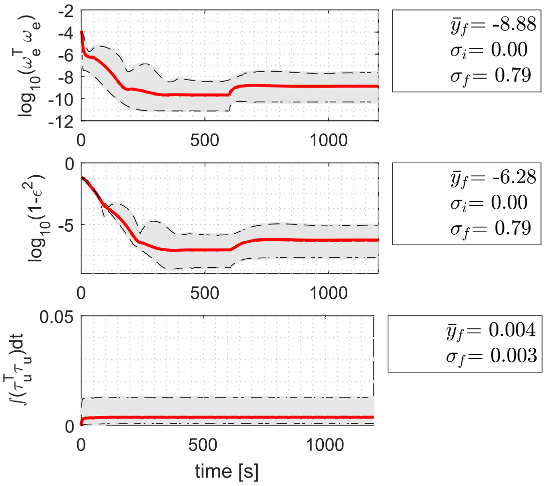

FIGURE 3 CIRAC gain sensitivity. Dashed lines highlight the envelope of simulations, the red full lines indicate the mean curves.

Figures 2 and 3 present all the simulations performed with IRAC and CIRAC respectively. DIRAC results are not reported with similar graphs as the difference with CIRAC simulations is minimal. For completeness, DIRAC results are included in Figure 4.

With σ_i and σ_f are identified the represented function standard deviation at the beginning and at the end of the simulation respectively, while $\bar{y}_f$ is the final mean value of the relative curve set. The first curve represents the CLF (16) relative to the angular velocity error ω_e and the second the attitude error CLF (3), both in logarithmic scale. The last one represents the effort of the controller with the integral of the squared norm of the commanded control action.

For both the IRAC and CIRAC cases, the wheel failure reflects in a slight but noticeable increase in the errors starting at $t = 600\,\mathrm{s}$. Both the CIRAC and DIRAC scheme (the latter not showed but exhibiting an analogous behavior) are then effective in counteracting actuator failures. Moreover, the lower mean final values (denoted by σ_f in Figures 2 and 3) of errors and control effort achieved by CIRAC with respect to IRAC denote a general better performance in the error/effort trade-off, while the reduced dispersion (highlighted by the gray area) hints a reduced sensitivity to parameter variation.

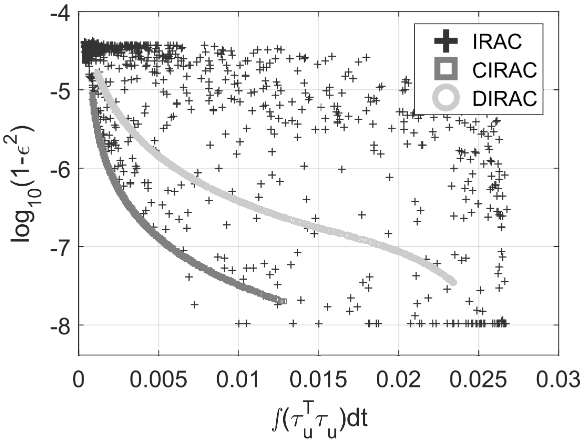

FIGURE 4 Gain sensitivity analysis: control effort vs final attitude error.

Figure 4 shows the variation of final attitude error with respect to the control effort at the variation of the tuning parameters. Thanks to the fact that only one single parameter needs to be tuned, for CIRAC and DIRAC the data points concentrate on a single curve, identifying a monotonic decreasing relationship between effort and error. Higher values of the gain rate adaptation parameter correspond to a faster system response and then to a lower error, as the relaxation factor is also multiplied by this gain. This behavior constitutes one of the major findings of this work, and it is a very attractive feature, in the context of a reliable industrial implementation: the system's sensitivity to the gain rate adaptation change is very simple to be extrapolated, enabling a fast tailoring of the algorithm to the specific problem.

On the contrary, IRAC presents a different behavior as data points are scattered on the whole domain, depending on 3 tunable constants. In general, a higher number of parameters corresponds to a larger flexibility in the adaptation to the specific problem. Nevertheless, the sensitivity to parameters change can be high and unpredictable, making difficult such tuning action. This is evident in Figure 4, where in most of the cases IRAC exhibits worse performances than CIRAC, except for a very few points, meaning that a very good performance with IRAC is attainable for some very specific combination of gains that may be difficult to find.

It can be seen that the CIRAC requires always a lower control effort than DIRAC regardless of the update gain. This is due to the fact that, in this specific simple case, the system dynamics on the 3 degrees of freedom are similar: the centralized approach is then capable to fully adapt to the system with an almost optimal control effort. On the contrary, in absence of relevant asymmetries in the inertia distribution, the decentralized approach requires a larger effort to achieve comparable accuracy. Such behavior is coherent with the theoretical development of DIRAC.

4.1.2 | Sensitivity to initial conditions

The robustness and convergence rate of the controllers is tested through simulations with initial attitude set randomly, spanning the whole attitude space with a uniform distribution. Time duration, wheel failure and the update of the reference attitude are kept identical to the previous case. The gains of the controllers are kept constant as per Table 2. Additional simulations are performed using a constant non adaptive controller, called for simplicity "MAX", with proportional gain set to the highest admissible value in the range of Table 1. MAX controller is introduced for comparison purposes, for it constitutes a boundary of the theoretical achievable performances in the effort/error space for linear feedback control.

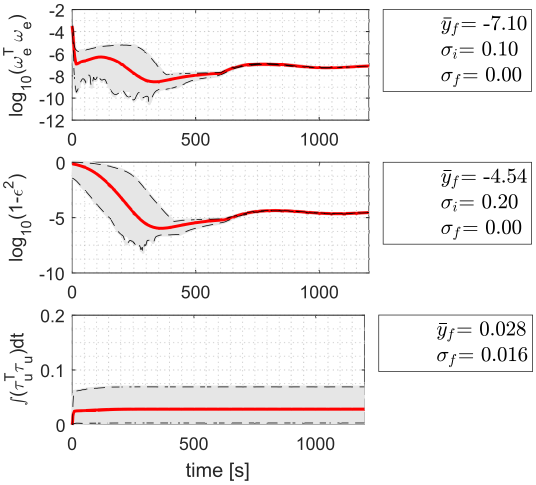

FIGURE 5 IRAC with different initial conditions. Dashed lines highlight the envelope of simulations, the red full lines indicate the mean curves.

Figures 5 and 6 show the behavior of IRAC and DIRAC with different initial conditions. CIRAC results are not reported as the difference with DIRAC is not highlighted by this representation. Again, actuator failure is visible in the errors' trend for all the controllers in a discontinuity at $t = 600$ s, efficaciously handled in all the cases.

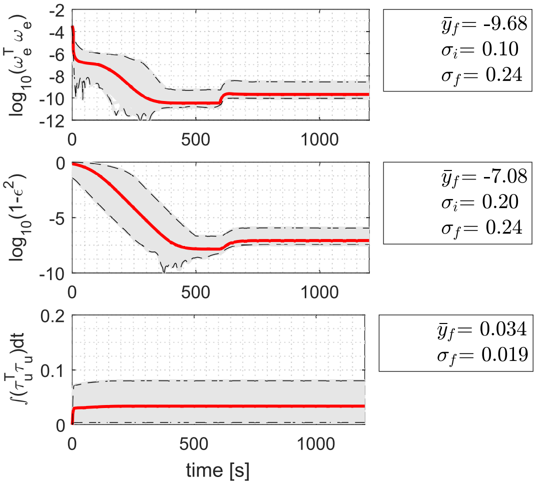

FIGURE 6 DIRAC with different initial conditions. Dashed lines highlight the envelope of simulations, the red full lines indicate the mean curves.

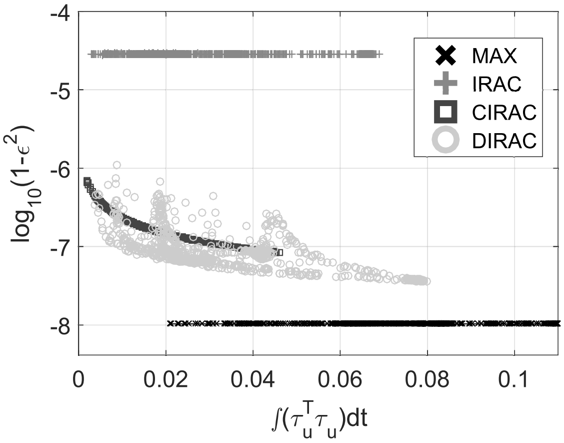

FIGURE 7 Effort vs final error with initial conditions variation.

Figure 5 presents the variability of the IRAC. The final achieved error is practically independent on the initial condition, with the system that converges to the same error norm in each simulation. Due to the nature of the boundaries, the selection of the gains is not always straightforward and might be re-assessed for different satellites. In any case, it is reasonable to conclude that once the gains of the controllers are set, the expected errors are quite predictable for any initial conditions.

The variability in the final error of the decentralized adaptive controller is shown in Figure 6. The decentralized approach induces a certain degree of variability, as the three different axis are exited in a different way depending on the initial condition.

Like in the previous case, Figure 7 represents each simulation as a point in the error-effort plane. As expected the IRAC follows a straight line, highlighting the convergence to a specific error and with effort depending on the initial attitude. The

MAX controller has a similar behavior: in terms of robustness this controller with no adaptation is able to deliver the lowest error possible at the price of the highest control effort.

On the other hand, the CIRAC variability is limited and predictable, and can be due to slower settling time with respect to IRAC. In this simulation the adaptive parameter has not been updated with a bias to settle for a specific error as otherwise described by Eq. (47). The decentralized version, DIRAC, has higher variability since, depending on the specific attitude, the path to convergence and excitation of the three axes is different. It worth to be noted that a very easy and quick tuning achieved a significantly lower error w.r.t. IRAC in all cases for both CIRAC and DIRAC. It is possible that the same performance could be still achievable by IRAC, but at the price of a more complex tuning activity with no guarantees of success.

4.1.3 | Steady state error analysis

We have seen that the CIRAC should be able, with the addition of a bias term in the update according to Eq. (32), to reach a user defined error $||\boldsymbol{e}||_{\mathrm{M}}$. To verify this claim, simulations with varying initial conditions are performed according to the previous scenario. The only modifications are the final time, which has been increased, and the absence of reaction wheel failure. This is done to highlight better the controlled system behavior with less variability induced by the fault.

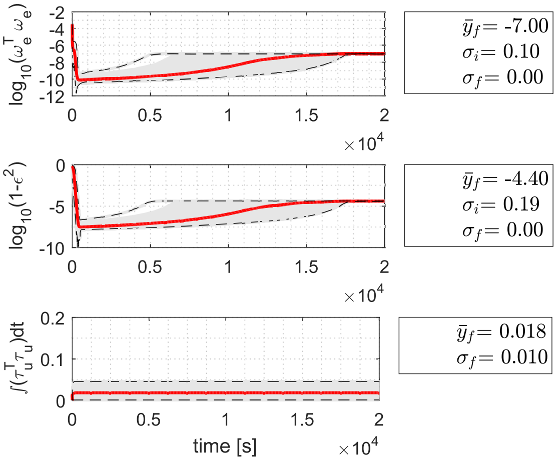

FIGURE 8 CIRAC steady state error test.

Results are presented in Figure 8 where it is easy to appreciate the convergence to the user defined velocity error $||\boldsymbol{e}||_{\mathrm{M}} = 10^{-3.5}$ after the initial transition period where the error is reduced to a minimum. $||\boldsymbol{e}||_{\mathrm{M}}$ represents the upper bound of the acceptable error: it can be seen that, after a stiffening phase, the system relaxes to acceptable levels. If disturbs, actuator faults or similar phenomena alter the equilibrium reached, as the error rises the system reacts again by increasing the value of f, corresponding to an increase in stiffness.

These results put in evidence the capability of CIRAC to relax the stiffening of the system to an acceptable value regardless of the initial condition and the input reference velocity.

4.2 | Orbital robotics test case

In order to show the ability of the DIRAC to increase performance and reducing the control effort while being robust to model uncertainties at the same time, a multibody simulation test campaign, representative of a practical class of problems, has been carried out. The reference scenario is a spacecraft designed for On Orbit Servicing applications, equipped with a robotic arm. The arm's end effector is required to be placed in a specific target pose relatively to the serviced satellite in a circular equatorial orbit. The context, the reference scenario, and the mathematical model for the multibody orbital robot can be found in Reference [43].

A 2D model is assumed: the spacecraft main body is equipped with a 3 links robotic manipulator and one reaction wheel for the attitude control. The total number of degrees of freedom is then 7 (3 for the spacecraft body, 3 for the robotic arm, and 1 for the reaction wheel). The system translation is controlled by a set of chemical thrusters with constant thrust and Sigma Delta Modulation[44]. The multibody implementation ensures the cross coupling effects of the different degrees of freedom. Disturbances are introduced by gravity effects and thrusters misalignment with respect to the center of mass, whose location changes as the arm moves. Measurement noises are not introduced. Relevant physical and control data are shown in Table 3.

TABLE 3 Planar robot data.

	base	wheel	link 1	link 2	link 3
Mass $\left[\text{kg}\right]$	1500.00	5.00	21.21	16.96	4.24
Inertia $\left[\text{kg} \cdot \text{m}^2\right]$	100.00	10.00	1.78	0.92	0.02
Characteristic lengths [m]	2.00	-	1.00	0.80	0.20
k_i	100.00	-	25.00	2.00	3.85
Joint lower limits $\left[\text{deg}\right]$	-	-	-180	-90	-90
Joint upper limits $\left[\text{deg}\right]$	-	-	0	90	90

This example is particularly suited to highlight the capabilities of DIRAC. The presence of a robotic arm implies a highly state-dependent matrix of inertia, changing as the system assumes different configurations.

Such a system is unsuitable for IRAC, which is heavily tailored to the attitude control problem and cannot be adapted to additional, robotic degrees of freedom without a deep work of reformulation. On the other hand, the formulation of CIRAC is sufficiently general to be adapted to such a system, but with an additional drawback. In fact, in case different parts of the system were characterized by very different dynamics, like in this example, the heavily centralized structure of CIRAC implies that the rate of adaptation is driven globally by the single tunable parameter. In such condition the system stiffness, determined by the global gain, will tend inevitably to increase following the "slowest" part, potentially leading to detrimental behavior and even instability, especially in case of real systems where the controller developed in a continuous framework is at a certain point implemented in a discrete fashion.

More complex centralized approaches could be possible, but at the price of modeling the system with high detail. Such detailed knowledge, especially for highly state-dependent matrix of inertia due to the presence of robotic appendages, is difficult to be obtained analytically, making the formulation of the dynamics in the form described by Eq. (14) really hard to achieve. Additional disadvantages of more complex schemes potentially include increase difficulty in tuning, due to the presence of a larger number of hyperparameters, and a more complex implementation, with corresponding higher computational demands (a critical aspect for all the space systems).

A decentralized approach avoids the necessity to compute the dynamics as a whole. The effect of the moving arm, from the decentralized attitude controller point of view, is equivalent to a time-varying disturbance on the inertia, modeled as $\boldsymbol{Ax}$ of Eq. (12), while the robotic harm itself is handled by its own, autonomous controller. By separating faster and slower dynamics in this way, DIRAC allows to retain the simplicity of CIRAC, matching at the same time the behavior of both the system parts while achieving a lower control effort. This capability of DIRAC to effectively handle complex systems, for which a centralized formulation would be arduous, without sacrificing tuning simplicity constitutes the second major finding of this work.

The performance of a DIRAC controller with respect to a basic, proportional, decentralized, non-adaptive controller is compared. The control under exam is applied to attitude and robotic joints degrees of freedom, while translation control is performed with the same standard, non-adaptive approach in both cases. Controllers are set to operate in velocity, meaning that the error is given by the difference of the state (platform angular velocity and joints angular velocity) with respect to the reference. Joints reference velocities are computed with a classical Jacobian transpose method preferred over generalized Jacobian/free floating approaches like the one expounded in Reference [36] for robustness issues. Thus, reference velocities are computed from the end effector velocity which is set to be the velocity that drives the end effector towards the target point. The construction is pretty similar to the guidance problem of the satellite, although here formulated in the 2D plane. As the target is relatively fixed, there is no need for a feedforward velocity term in the controllers. In both controllers setting, the reference inertia of link 2 has been deliberately underestimated to highlight the capability of the proposed controller to compensate errors due to uncertainties. The control cycle is set to 100 Hz sampling rate. The rendezvous approach is on v-bar, meaning the direction where the relative drift due to orbital motion is lower[45].

The comparison between the proposed adaptive scheme and the basic proportional controller compares the attitude error using $V_\varepsilon\left(\mathbf{q}_e\right)$ as metric and a cost function of the robotic arm tip position and attitude error. Additionally, the orbital robot base angular velocity error and the arm joints velocity errors are compared. Finally, the energy cost of both controllers is compared by looking at the reaction wheel speed and the integral of the control torques used to move the robotic arm towards its goal.

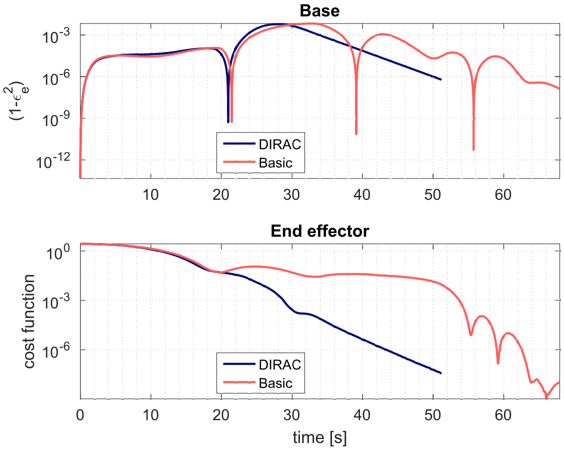

FIGURE 9 Attitude and robotics pose errors.

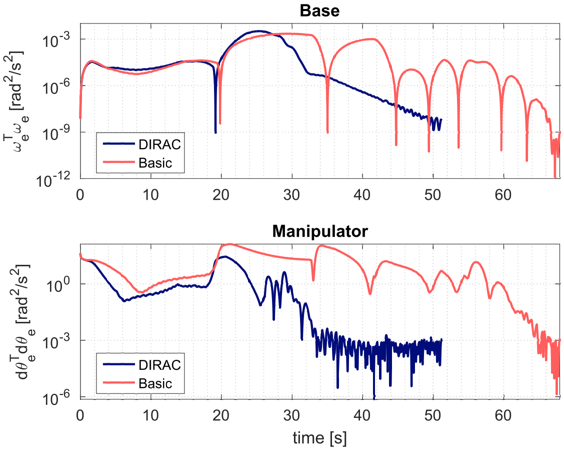

FIGURE 10 Attitude and robotics rotational rate errors.

Figures 9 and 10 show the differences about the attitude error, the cost function of the robotic arm (that comprehends relative position and attitude of the end effector), and the rotational rate errors relative to the satellite body and the robotic arm joints. The adaptive controller is able to achieve the objective faster than the basic controller by overcoming the underestimation of a parameter. Given enough time the basic proportional controller is able to achieve same results. Should be noted that using a much slower reference trajectory the difference between the two controllers would be reduced.

The DIRAC is able to overcome uncertainties and reduce the errors significantly faster than the baseline, with less oscillations in the transient phase. Plus, another major improvement of DIRAC with respect to the standard controller is the reduced control effort, shown in Figure 11 in terms of reaction wheel speed and cumulative joints control effort. This effect is due not only to the faster maneuver, but also to the decrease of the proportional gain actuated by the DIRAC in the final phases.

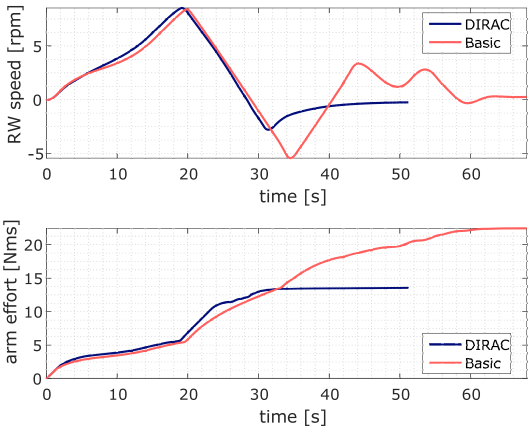

FIGURE 11 Control effort.

5 | CONCLUSIONS

In this paper two new attitude controllers, tailored for spacecraft attitude control and belonging to the indirect robust adaptive controller class, are developed in centralized and decentralized form. Improved ease of tuning, thanks to the dependence on one single tunable constant, and a reduced variability with respect to problem-specific parameters constitute the main advantages of the new formulation, with consequently shorter development time and higher confidence in system verification, when applied in practice onboard actual space systems. Both versions are able to relax the system stiffness up to an user defined error threshold, making the controller robust to hyper-stiffening, and easing the tailoring to specific mission requirements, in a simple trade-off between control error and effort. Uniform Ultimate Boundedness convergence is theoretically demonstrated for both the controllers, while a simulation campaign, representative of a real case of application, confirmed good properties of convergence, performance, and sensitivity with respect to the proportional gain, with a reduced control effort. The scheme proved to be robust to actuators fault and incorrect estimation of system parameters, while the simple control structure, with consequently low computational burden, enables its application to a wide range of systems. A simulation of an orbital robot case proved the effectiveness of the decentralized version of the controller in handling also more complex systems with several degrees of freedom and highly state-dependent moments of inertia. All these properties make the proposed algorithms very appealing for the new arising wave of space applications.

CONFLICT OF INTEREST

The authors declared that they have no conflicts of interest for this article.

DATA AVAILABILITY STATEMENT

Data sharing is not applicable to this article as no datasets were generated or analyzed during the current study.

ORCID

Aureliano Rivolta: https://orcid.org/0000-0003-0832-0431

Paolo Lunghi: https://orcid.org/0000-0002-9501-1049

References

1. Rivolta A, Lunghi P, Lavagna M. GNC & robotics for on orbit servicing with simulated vision in the loop. *Acta Astronautica* 2019; 162: 327–335. doi: 10.1016/j.actaastro.2019.06.005
2. Moghaddam BM, Chhabra R. On the guidance, navigation and control of in-orbit space robotic missions: A survey and prospective vision. *Acta Astronautica* 2021; 184: 70–100. doi: 10.1016/j.actaastro.2021.03.029
3. Luu M, Hastings DE. Review of On-Orbit Servicing Considerations for Low-Earth Orbit Constellations. In: ASCEND 2021. AIAA. ; 2021
4. Cinelli M, Puccetti S, Lavagna M, Lunghi P, Pucacco G. High Energy Modular Ensemble of Satellites Mission: Towards the final Full Constellation. *Acta Astronautica* 2021; 189: 129–142. doi: 10.1016/j.actaastro.2021.08.024
5. Benvenuto R, Lunghi P, Pesce V, et al. Parabolic flight experiment to validate tethered-tugs dynamics and control for reliable space transportation applications. In: 67th International Astronautical Congress (IAC). IAF. ; 2016; Guadalajara, Mexico.
6. Krstic M, Tsiotras P. Inverse optimal stabilization of a rigid spacecraft. *IEEE Transactions on Automatic Control* 1999; 44(5): 1042–1049. doi: 10.1109/9.763225
7. Loquen T, Plinval dH, Cumer C, Alazard D. Attitude control of satellites with flexible appendages: a structured H_∞ control design. In: AIAA Guidance, Navigation, and Control Conference. American Institute of Aeronautics and Astronautics. ; 2012
8. Menezes EF, Aguiar RS, Simões AM, Apkarian P. Structured robust controller design via non-smooth mixed μ synthesis. *IET Control Theory & Applications* 2016; 10(17): 2186–2193. doi: 10.1049/iet-cta.2016.0570
9. Ahmed J, Coppola VT, Bernstein DS. Adaptive asymptotic tracking of spacecraft attitude motion with inertia matrix identification. *Journal of Guidance Control and Dynamics* 1998; 21(5): 684–691. doi: 10.2514/6.1997-3530

10. Costic B, Dawson D, De Queiroz M, Kapila V. Quaternion-based adaptive attitude tracking controller without velocity measurements. *Journal of Guidance, Control, and Dynamics* 2001; 24(6): 1214–1222. doi: 10.2514/3.22618

11. Lavretsky E, Wise KA. Robust adaptive control. In: Robust adaptive control. Advanced Textbooks in Control and Signal Processing. London: Springer. 2013 (pp. 317–353)

12. Luo W, Chu YC, Ling KV. Inverse optimal adaptive control for attitude tracking of spacecraft. *IEEE Transactions on Automatic Control* 2005; 50(11): 1639–1654. doi: 10.1109/tac.2005.858694

13. Shi K, Liu C, Sun Z, Yue X. Coupled orbit-attitude dynamics and trajectory tracking control for spacecraft electromagnetic docking. *Applied Mathematical Modelling* 2022; 101: 553–572. doi: 10.1016/j.apm.2021.08.030

14. Shi K, Liu C, Biggs JD, Sun Z, Yue X. Observer-based control for spacecraft electromagnetic docking. *Aerospace Science and Technology* 2020; 99: 105759. doi: 10.1016/j.ast.2020.105759

15. Cai W, Liao X, Song Y. Indirect robust adaptive fault-tolerant control for attitude tracking of spacecraft. *Journal of Guidance, Control, and Dynamics* 2008; 31(5): 1456. doi: 10.2514/1.31158

16. Boškovic JD, Li SM, Mehra RK. Robust adaptive variable structure control of spacecraft under control input saturation. *Journal of Guidance, Control, and Dynamics* 2001; 24(1): 14–22. doi: 10.2514/2.4704

17. Boskovic JD, Li SM, Mehra RK. Robust tracking control design for spacecraft under control input saturation. *Journal of Guidance, Control, and Dynamics* 2004; 27(4): 627–633. doi: 10.2514/1.1059

18. Xiao B, Hu Q, Zhang Y. Adaptive sliding mode fault tolerant attitude tracking control for flexible spacecraft under actuator saturation. *IEEE Transactions on Control Systems Technology* 2012; 20(6): 1605–1612. doi: 10.1109/tcst.2011.2169796

19. Zou AM, Kumar KD, Ruiter dAHJ. Robust attitude tracking control of spacecraft under control input magnitude and rate saturations. *International Journal of Robust and Nonlinear Control* 2016; 26(4): 799–815. doi: 10.1002/rnc.3338

20. Jiang Y, Hu Q, Ma G. Adaptive backstepping fault-tolerant control for flexible spacecraft with unknown bounded disturbances and actuator failures. *ISA transactions* 2010; 49(1): 57–69. doi: 10.1016/j.isatra.2009.08.003

21. Shao X, Hu Q, Guo L. Adaptive spacecraft attitude tracking control with guaranteed transient performance. In: 36th Chinese Control Conference (CCC). IEEE. ; 2017: 9442–9447

22. Gui H, Vukovich G. Adaptive fault-tolerant spacecraft attitude control using a novel integral terminal sliding mode. *International Journal of Robust and Nonlinear Control* 2017; 27(16): 3174–3196. doi: 10.1002/rnc.3733

23. Hu Q, Huo X, Xiao B. Reaction wheel fault tolerant control for spacecraft attitude stabilization with finite-time convergence. *International Journal of Robust and Nonlinear Control* 2013; 23(15): 1737–1752. doi: 10.1002/rnc.2924

24. Amrr SM, Sarkar R, Banerjee A, Saidi AS, Nabi Mu. Fault-tolerant finite-time adaptive higher order sliding mode control with optimized parameters for attitude stabilization of spacecraft. *International Journal of Robust and Nonlinear Control* 2021; in press(n/a). doi: 10.1002/rnc.5934

25. Tao M, Chen Q, He X, Sun M. Adaptive fixed-time fault-tolerant control for rigid spacecraft using a double power reaching law. *International Journal of Robust and Nonlinear Control* 2019; 29(12): 4022–4040. doi: 10.1002/rnc.4593

26. Shen Q, Wang D, Zhu S, Poh EK. Inertia-free fault-tolerant spacecraft attitude tracking using control allocation. *Automatica* 2015; 62: 114–121. doi: 10.1016/j.automatica.2015.09.027

27. Li Y, Ye D, Sun Z. Robust finite time control algorithm for satellite attitude control. *Aerospace Science and Technology* 2017; 68: 46–57. doi: 10.1016/j.ast.2017.05.014

28. Huo M, Huo X, Karimi HR, Ni J. Finite-time control for attitude tracking maneuver of rigid satellite. *Abstract and Applied Analysis* 2014; 2014. doi: 10.1155/2014/302982

29. Prajna S, Parrilo PA, Rantzer A. Nonlinear control synthesis by convex optimization. *IEEE Transactions on Automatic Control* 2004; 49(2): 310–314. doi: 10.1109/tac.2003.823000

30. Ebenbauer C, Allgöwer F. Analysis and design of polynomial control systems using dissipation inequalities and sum of squares. *Computers & chemical engineering* 2006; 30(10-12): 1590–1602. doi: 10.1016/j.compchemeng.2006.05.014

31. Kristiansen R, Nicklasson PJ, Gravdahl JT. Satellite Attitude Control by Quaternion-Based Backstepping. *IEEE Transactions on Control Systems Technology* 2009; 17(1): 227-232. doi: 10.1109/TCST.2008.924576

32. Kristiansen R, Nicklasson PJ, Gravdahl JT. Spacecraft coordination control in 6DOF: Integrator backstepping vs passivity-based control. *Automatica* 2008; 44(11): 2896–2901. doi: 10.1016/j.automatica.2008.04.019

33. Ali I, Radice G, Kim J. Backstepping control design with actuator torque bound for spacecraft attitude maneuver. *Journal of guidance, control, and dynamics* 2010; 33(1): 254–259. doi: 10.2514/1.45541

34. Bhat SP, Bernstein DS. A topological obstruction to continuous global stabilization of rotational motion and the unwinding phenomenon. *Systems & Control Letters* 2000; 39(1): 63–70. doi: 10.1016/s0167-6911(99)00090-0

35. Mayhew CG, Sanfelice RG, Teel AR. Robust global asymptotic attitude stabilization of a rigid body by quaternion-based hybrid feedback. In: Proceedings of the 48th IEEE Conference on Decision and Control. IEEE. ; 2009: 2522–2527

36. Umetani Y, Yoshida K. Resolved motion rate control of space manipulators with generalized Jacobian matrix. *IEEE Transactions on robotics and automation* 1989; 5(3): 303–314. doi: 10.1109/70.34766

37. Bakule L. Decentralized control: An overview. *Annual Reviews in Control* 2008; 32(1): 87–98. doi: 10.1016/j.arcontrol.2008.03.004

38. Siljak DD. *Decentralized Control of Complex Systems*. Boston, MA: Academic Press . 1991.

39. Tsiotras P. Further passivity results for the attitude control problem. *IEEE Transactions on Automatic Control* 1998; 43(11): 1597–1600. doi: 10.1109/9.728877

40. Wie B. *Space Vehicle Dynamics and Control*. Reston, VA: AIAA . 2008.

41. Dodge FT. *The New Dynamic Behavior of Liquids in Moving Containers*. San Antonio, TX: South West Research Institute . 2000.

42. Lunghi P, Masarati P, Lavagna M. Multibody modeling of sloshing in spacecraft ascent and landing maneuvers. In: ASME 2016 IDETC/CIE - International Design Engineering Technical Conferences & Computers and Information in Engineering Conference. ASME. ; 2016; Charlotte, NC

43. Rivolta A. *Guidance Navigation Control And Robotics For On Orbit Servicing*. PhD thesis. Politecnico di Milano, Milan, Italy; 2018.

44. Zappulla R, Virgili-Llop J, Romano M. Spacecraft Thruster Control via Sigma–Delta Modulation. *Journal of Guidance, Control, and Dynamics* 2017: 1–6. doi: 10.2514/1.g002986

45. Fehse W. *Automated Rendezvous and Docking of Spacecraft*. Cambridge Aerospace SeriesCambridge University Press . 2003